Influence of secondary ligand on structures and topologies of lanthanide coordination polymers with 1,3,5-triazine-2,4,6-triamine hexaacetic acid

Bunlawee Yotnoi[†], Natthaya Meundaeng[†], Watcharee Funfuenha[†], Mookda Pattarawarapan[†], Timothy J. Prior[‡] and Apinpus Rujiwatra*[†]

[†]Department of Chemistry, Faculty of Science, Chiang Mai University, Chiang Mai 50200, Thailand

[‡]Department of Chemistry, University of Hull, Kingston upon Hull, HU6 7RX, UK

∗ Corresponding author:

Department of Chemistry, Faculty of Science,

Chiang Mai University,

Chiang Mai 50200

Thailand

Telephone: +66 5394 1906

Fax: +66 5389 2277

E-mail: apinpus.rujiwatra@cmu.ac.th

Influence of secondary ligand on structures and topologies of lanthanide coordination polymers with 1,3,5-triazine-2,4,6-triamine hexaacetic acid

Bunlawee Yotnoi[†], Natthaya Meundaeng[†], Watcharee Funfuenha[†], Mookda Pattarawarapan[†], Timothy J. Prior[‡] and Apinpus Rujiwatra*[†]

[†]Department of Chemistry, Faculty of Science, Chiang Mai University, Chiang Mai 50200, Thailand

[‡]Department of Chemistry, University of Hull, Kingston upon Hull, HU6 7RX, UK

Abstract

A series of new lanthanide coordination polymers have been synthesized and structurally characterized; $[Ln_4(TTHA)_2(pzac)(H_3O)_2(H_2O)]\cdot5H_2O$ (Ln = Pr (**Ia**) and Nd (**Ib**)), $[Sm_8(TTHA)_4(pzac)_{0.5}(H_3O)(H_2O)_{7.5}]\cdot4H_2O$ (**II**), $[Ln_4(HTTHA)_2(SO_4)(H_2O)_4]\cdot5H_2O$ (Ln = Pr (**IIIa**) and Nd (**IIIb**)), where H_6TTHA = 1,3,5-triazine-2,4,6-triamine hexaacetic acid, and H_2pzac = 2,5-dioxo-piperazine-1,4-diacetic acid. The compounds feature three-dimensional frameworks comprising the deprotonated H_6TTHA as the primary ligand and either the *in situ* generated $pzac^{2-}$ or the sulfate as the secondary ligands. The influence of the deprotonated H_6TTHA in directing the framework structures through the preferential coordination modes and molecular conformation is illustrated and described. The effect of the secondary ligands in increasing the compactness of the frameworks and in the alternation of the framework topologies based on the four-connected cooperate **pts** type is described.

Keywords: Coordination polymer; Lanthanide; Polycarboxylate; Crystal structure; Topology

1. Introduction

In the design of coordination polymers and metal-organic frameworks, great attention has been paid to the employment of triazine-based polycarboxylate ligands, *e.g.* 1,3,5-tris(4-pyridyl)triazine [1], 4,6-bis(4-pyridyl)-1,3,5-triazin-2-ol [2], 2,4,6-tri(2-pyridyl)-1,3,5-triazine [3], and *N*,*N'*,*N''*-1,3,5-triazine-2,4,6-triyltris-glycine [4], by virtue of their versatile coordination modes and excellent coordination ability. Among ligands of this type, there are surprisingly few reports on the use of the highly symmetrical 1,3,5-triazine-2,4,6-triamine hexaacetic acid (H_6TTHA; Scheme 1) which should be beneficial in framework design. Six flexible $-N(CH_2COOH)_2$ arms which are readily available for coordination can be tailored for varying degrees of deprotonation and therefore number of coordinating carboxylate groups. Since the first report of this ligand over a decade ago [5], less than twenty structures have been reported to the Cambridge Structure Database [6]. Among the rare examples of coordination polymeric frameworks derived from deprotonated H_6TTHA, almost all of the metals of choices are the transition metals [7-12]. According to literature, smaller ligands such as pyridinium-4-thiolate [8], 4,4'-dipyridylsulfide [8], and 2,2'-bipyridine [11] have been applied in an attempt to modulate the derived frameworks. To the best of our knowledge, there is only one series of isostructural coordination polymers to date which are constructed from the lanthanide metals and H_6TTHA, *i.e.* $[Ln^{III}_2(TTHA)(H_2O)_4]\cdot9H_2O$ where Ln = Sm, Eu, Tb, Gd and Dy [13,14]. These lanthanide coordination polymers are three-dimensional in nature of over 30% void [13,14].

Following our interest in the use of H_6TTHA in the fabrication of lanthanide coordination polymers, the early lanthanides including Pr, Nd and Sm have been attempted. Considering the coordination ability and capability in forming hydrogen bonds with H_6TTHA, the sulfate salts of the lanthanides have been employed in order to provide the possibility for the incorporation of sulfate into the frameworks. According to literature [15],

the generation of smaller secondary ligands from H_6TTHA under the synthesis conditions employed may also be expected. This may introduce diversity to the constructed frameworks.

Here, the syntheses and single crystal structures of a series of new lanthanide coordination polymers, including [Ln$_4$(TTHA)$_2$(pzac)(H$_3$O)$_2$(H$_2$O)]·5H$_2$O (Ln = Pr (**Ia**) and Nd (**Ib**)), [Sm$_8$(TTHA)$_4$(pzac)$_{0.5}$(H$_3$O)(H$_2$O)$_{7.5}$]·4H$_2$O (**II**), and [Ln$_4$(HTTHA)$_2$(SO$_4$)(H$_2$O)$_4$]·5H$_2$O (Ln = Pr (**IIIa**) and Nd (**IIIb**) where pzac^{2-} = 2,5-dioxo-piperazine-1,4-diacetate (Scheme 1) which are *in situ* generated, are reported. A common building block for these coordination polymers is identified. The influence of secondary ligands, *i.e.* sulfate and pzac^{2-}, in modulating the derived frameworks is discussed. Topological relation between the title frameworks and the 4-connected **pts** net of [Ln$^{III}_2$(TTHA)(H$_2$O)$_4$]·9H$_2$O [13,14] is described.

2. Experimental

2.1. Materials and methods

Ln$_2$(SO$_4$)$_3$·8H$_2$O (Ln = Pr, Nd and Sm) were crystallized from solutions of Pr$_6$O$_{11}$ (TJTM, 99%), Nd$_2$O$_3$ (TJTM, 99%) and Sm$_2$O$_3$ (TJTM, 99%), accordingly, in 0.10 M H$_2$SO$_4$ aqueous solution. The amounts of water of crystallization were determined by thermogravimetric analyses. 1,3,5-triazine-2,4,6-triamine hexaacetic acid (C$_{15}$H$_{18}$N$_6$O$_{12}$, H$_6$TTHA) was prepared and characterized according to literature [16]. The NMR data of the H$_6$TTHA ligand is provided as supplementary information. The 2,5-dioxo-piperazine-1,4-diacetate (C$_8$H$_7$N$_2$O$_6$, pzac^{2-}) was generated *in situ* under hydrothermal synthesis conditions. Elemental analyses were performed with Perkin Elmer PE2400 Series II CHNS/O Analyzer. The IR spectra were collected from samples prepared as KBr pellets (BDH, 98.5%, dilution *ca.* 1:20) from 4000-400 cm^{-1} using Bruker Tensor 27 FT-IR spectrometer. The powder X-ray diffraction data were

collected using the Bruker D2 Phaser diffractometer (Cu $K\alpha$ radiation, $\lambda = 1.54060$ Å, 30 kV and 10 mA).

2.2. Syntheses of Ia, Ib and II

Green crystals of $[Pr_4(TTHA)_2(pzac)(H_3O)_2(H_2O)]\cdot5H_2O$ (**Ia**) were prepared from the reaction of $Pr_2(SO_4)_3\cdot8H_2O$ (0.2200 g, 0.30 mmol) and H_6TTHA (0.2418 g, 0.50 mmol) in 10.0 mL of deionized water. The reaction was conducted under hydrothermal conditions generated at 180 °C for 72 h, using 23 mL PTFE lined autoclave. After the reaction was cooled down to room temperature, the crystals were filtered and dried. Purple crystals of $[Nd_4(TTHA)_2(pzac)(H_3O)_2(H_2O)]\cdot5H_2O$ (**Ib**) and yellow crystals of $[Sm_8(TTHA)_4(pzac)_{0.5}(H_3O)(H_2O)_{7.5}]\cdot4H_2O$ (**II**) were prepared using similar procedures, employing $Nd_2(SO_4)_3\cdot8H_2O$ (0.2200 g, 0.30 mmol) and $Sm_2(SO_4)_3\cdot8H_2O$ (0.2250 g, 0.30 mmol) accordingly. The pH of each reaction mixture was measured using Merck pH indicator strips, indicating the same range of acidic pH (3 to 4). Since only a few crystals were obtained for each synthesis, further investigation on physical properties was not possible.

Anal. Calcd. (%) for $C_{38}H_{47}N_{14}O_{38}Pr_4$ (**Ia**): C, 24.39; H, 2.53; N, 10.48. Found: C, 19.38; H, 2.43; N, 9.07 %. IR (KBr, cm^{-1}): 3472s, 2935w, 1882w, 1627m, 1553vs, 1487s, 1432s, 1400s, 1300vs, 1197m, 991m, 902w, 821m, 748m, 613s, 539w.

Anal. Calcd. (%) for $C_{64}H_{76.5}N_{25}O_{63.5}Sm_8$ (**II**): C, 22.51; H, 2.26; N, 10.25. Found: C, 22.54; H, 2.64; N, 10.14. IR (KBr, cm^{-1}): 3472s, 2935w, 1851w, 1635m, 1553vs, 1487s, 1435s, 1401s, 1299vs, 1198m, 991m, 902w, 821m, 748m, 614s, 538w.

2.3. Syntheses of IIIa and IIIb

In the preparation of $[Pr_4(HTTHA)_2(SO_4)(H_2O)_4]\cdot5H_2O$ (**IIIa**), the hydrothermal reaction between $Pr_2(SO_4)_3\cdot8H_2O$ (0.2200 g, 0.30 mmol) and H_6TTHA (0.1400 g, 0.3 mmol) was

conducted under autogenous pressure generated at 180 °C, using 10.0 mL deionized water and 23 mL PTFE lined autoclave. The reaction was cooled down after 48 h, giving green crystals of **IIIa**. The same chemical stoichiometry and hydrothermal condition were adopted in the preparation of $[Nd_4(HTTHA)_2(SO_4)(H_2O)_4]\cdot 5H_2O$ (**IIIb**) using $Nd_2(SO_4)_3.8H_2O$ (0.2200 g, 0.30 mmol). The attempt to use $Sm_2(SO_4)_3.8H_2O$ (0.2250g, 0.30 mmol) resulted in the previously reported compound, $[Sm_2(TTHA)(H_2O)_4]\cdot 9H_2O$ (**IV**) [14]. The pH of each reaction mixture was measured using Merck pH indicator strips, revealing the pH values of 4-5. Due to the fact that only a few crystals were obtained for each synthesis, it was not possible to carry out further investigation on physical properties.

Anal. Calcd. (%) for $C_{30}H_{44}N_{12}O_{36}Pr_4S$ (**IIIa**): C, 20.66; H, 2.54; N, 9.64. Found: C, 20.39; H, 2.47; N, 9.53. IR (KBr, cm^{-1}): 3456s, 2935w, 1843w, 1621m, 1550vs, 1487s, 1439s, 1385s, 1300vs, 1192m, 1097s, 991m, 886w, 821m, 723m, 609s, 540w.

2.4. Single crystal structures determination

Intensity data sets of **Ia**, **II** and **IIIa** were collected in series of ω-scans using a Stoe IPDS2 image plate diffractometer and Mo $K\alpha$ radiation at 150(2) K in an Oxford Cryosystems nitrogen gas cryostream. The collected data were corrected for absorption using the Tompa method [17]. The single crystal data of **Ib** and **IIIb**, which are isostructural to **Ia** and **IIIa**, respectively, were collected on a Bruker SMART Apex CCD diffractometer at 293(2) K. All structures were solved by direct methods within SHELXS-97 [18] and full-matrix least squares refinement carried out within SHELXL-97 [18] *via* the WinGX program interface [19]. All non-hydrogen positions were located in the direct and difference Fourier maps and refined using anisotropic displacement parameters. The hydrogen atoms of the organic moieties were apparent from difference Fourier maps and refined using the riding mode. Summary of the crystallographic data and refinement parameters is given in Table 1. Powder X-ray diffraction

data (see supplementary information) affirmed the crystals to be representatives of the yielded samples and therefore their purities.

Crystallographic analysis was complicated by the generation of the pzac^{2-} ligand *in situ* and the fact that each structure studied displays disorder in the secondary ligand set. In each case the secondary ligand (sulfate or pzac^{2-}) lies close to a center of inversion and it can be difficult to identify clearly exactly which species are present. Difference Fourier maps prove extremely useful in unravelling problems of this type. For each of the unique structures, the disorder is described in detail and pictures to show the nature of disorder are found in the supplementary information.

3. Results and Discussion

3.1. Hydrothermal syntheses and *in-situ* generation of secondary organic ligand

A series of new lanthanide coordination polymers of four distinct frameworks have been synthesized from the hydrothermal reactions of $Ln_2(SO_4)_3 \cdot 8H_2O$ (Ln = Pr, Nd and Sm) and H_6TTHA by a careful modification of the reactant mole ratios and the hydrothermal reaction time. The use of an equimolar ratio of the starting reagents and a reaction time of 48 h resulted in a framework containing either the partially deprotonated HTTHA^{5-} and the sulfate anions (**IIIa** and **IIIb**) or the fully deprotonated TTHA^{6-} anion ([Sm$_2$(TTHA)(H$_2$O)$_4$]·9H$_2$O [14]). The prolongation of the reaction time to 72 h and the use of excess H_6TTHA in the syntheses of **Ia**, **Ib** and **II** however resulted in the generation of only the fully deprotonated TTHA^{6-} and the dicarboxylate pzac^{2-} anions. According to literature, the pzac^{2-} anion can be *in situ* generated under acidic hydrothermal conditions from the cyclodehydration reaction of iminodiacetic acid, which could be also *in situ* generated from the decomposition of H_6TTHA [15].

3.2. Structural description of Ia and Ib

Since compounds **Ia** and **Ib** are isostructural, the crystal structure of **Ia** which is deduced from low temperature data will be described. The asymmetric unit of **Ia** comprises two distinct Pr ions, a fully deprotonated TTHA^{6-}, a fraction of pzac^{2-}, and three unbound water molecules (Figure 1). The Pr1 is surrounded by nine O atoms (O1, 2×O2, O5, O6, O8, O10, O11 and O12) from four TTHA^{6-} to form a square-face capped square antiprismatic *SAPRS*-{PrO$_9$} unit. Pr2 is coordinated to seven O atoms (2×O3, O4, O6, O7, O8 and O9) from three TTHA^{6-}, leaving space to be completed by the chelating O14–C16–O15 of pzac^{2-} and the water O13. The coordination of Pr2 is thus ten-fold and characterized by a square-face bicapped square antiprismatic *SAPRS*-{PrO$_{10}$}. Owing to the substitutional disorder at the chelating O14 and O15 of pzac^{2-} with O16 of the other water molecule, the *SAPRS*-{PrO$_{10}$} is partially replaced by a nine-fold distorted tricapped triangular prismatic *TPRS*-{PrO$_9$}. Given the equal occupancies of 50% for the two disordered components, amounts of the *SAPRS*-{PrO$_{10}$} and *TPRS*-{PrO$_9$} units are equal.

In the construction of the framework structure in **Ia**, two equivalent *SAPRS*-{PrO$_9$} units of Pr1 are bridged by 2×O1–C1–O2 and 2×O11–C11–O12 of TTHA^{6-} to form an edge-sharing {Pr$_2$O$_{16}$} dimer as depicted in Figure 2(a). Details on modes of coordination exhibited by the organic anions and the metal ions bridged by each carboxylate are summarized in Table 2. A dimer of Pr2 is likewise built up by joining two successive *SAPRS*-{PrO$_{10}$}/*TPRS*-{PrO$_9$} units using 2×O4–C3–O3 bridges of TTHA^{6-}. Two unique dimers are condensed further in a regular alternating sequence by O5–C5–O6, O7–C7–O8 and O9–C9–O10 of TTHA^{6-}, to form a corrugated edge-sharing chain extending along the [1 5 -9] direction. Distances between the successive Pr ions in the chain vary from 4.0686(7) Å to 4.3542(6) Å. These chains are bundled up in a hexagonal array fashion by the chelating pzac^{2-} and TTHA^{6-} using two common μ_2-η^1:η^1-OCO and μ_2-η^1:η^2-OCO bridges as shown in Figure 2(b). While each TTHA^{6-} joins three neighboring chains through seven Pr ions, the pzac^{2-} links two *SAPRS*-

{Pr_2O_{18}} dimers of two adjacent chains, which can alternatively viewed as the other infinite one-dimensional zigzag chain. As a result of such a dense packing, the framework of **Ia** contains an almost negligible void volume of 5.3% calculated using PLATON [20]. Located in the void is water of crystallization. These water molecules establish O-H···O, N–H···O, and C–H···O hydrogen bonding interactions with the framework as listed in Table 3.

According to the single crystal data, the ratio of Pr-to-TTHA^{6-}-to-pzac^{2-} is 4:2:1. If every Pr ion is in the most stable trivalent state (Pr^{III}), this ratio would lead to a -2 charge on the framework which is not chemically sensible. In order to yield a neutral compound, the excess negative charges need to be counterbalanced. Three assumptions can be contemplated; (i) the coexistence of Pr^{III} and Pr^{IV} in 1:1 ratio which will bring about the neutral [Pr$^{III}_2$Pr$^{IV}_2$(TTHA)$_2$(pzac)(H$_2$O)$_3$]·5H$_2$O, (ii) the protonation at one of the N atoms of −N(CH$_2$COO)$_2$ which will result in the presence of HTTHA^{5-} anion and therefore the neutral [Pr$^{III}_4$(HTTHA)$_2$(pzac)(H$_2$O)$_3$]·5H$_2$O, and (iii) the presence of two hydronium ions in the formula which will lead also to the neutral [Pr$^{III}_4$(TTHA)$_2$(pzac)(H$_3$O)$_2$(H$_2$O)]·5H$_2$O. In order to validate the valence of Pr ions, bond valence sums (BVSs) [21] were calculated. According to the calculated BVSs of 3.43 and 3.63 for Pr1, and 3.43 for Pr2, the tetravalent state cannot be assumed for Pr2. Regarding the protonation at N atom of the −N(CH$_2$COO) arms, the sum of ∠CNC about each N, *i.e.* N1 355.8(4)°, N2 359.3(4)° and N3 359.2(4)°, which is close to 360° suggest the perfect triangular planar geometry. The protonation at one of these sites is therefore unlikely. The presence of H$_3$O$^+$ ions is by far the most probable, and is suggested by a significantly long bond distance of Pr2–O13 (2.516(5) Å), relative to Pr2–O16 (2.451(11) Å) and those of other relevant compounds in which the ligands are water [22-24]. The presence of absorption at *ca.* 1800 cm^{-1} in the IR spectra (see supplementary information) is additionally in favor for the existence of H$_3$O$^+$ [25,26]. The chemical formula [Nd$^{III}_4$(TTHA)$_2$(pz-

2OAc)(H$_3$O)$_2$(H$_2$O)]·5H$_2$O can be similarly assumed for **Ib**, and is consistent with literature reports of the different bond lengths for Nd–OH$_2$ and Nd–OH$_3$ [27-29].

3.3. Structural description of II

The asymmetric unit of **II** consists of four unique Sm ions, two molecules of TTHA^{6-}, half a molecule of pzac^{2-}, and water of crystallization (Figure 3). All of the Sm ions are present as a nine-fold coordinate square-face monocapped antiprismatic geometry, *SAPRS*-{SmO$_9$}, but with varied degree of hydration. In addition to eight O atoms (O1, O2, O3, 2×O4 O7 and O8) from three TTHA^{6-}, the *SAPRS*-{SmO$_9$} unit of Sm1 is completed by the waters O5 and O6. Sm2 and Sm3 are similarly surrounded by nine O atoms from four TTHA^{6-} without the coordinating water molecule (Sm2: O2, O7, O9, O10, O11, O12, O13, O14 and O15; Sm3: O10, O14, O16, O17, O18, O19, O20, O21 and O22).

The coordination about Sm4 is complicated by crystallographic disorder. In addition to six O atoms (O20, O22, O23, O24, O26 and O27) from three TTHA^{6-} and the water O25 atom, the *SAPRS*-{SmO$_9$} unit of Sm4 is completed by either two water molecules (O28 and O29B) or by bidentate carboxylate from the pzac^{2-} ligand (O28 and O29A). Each of these arrangements is present in 50% of the Sm4 sites. We see no evidence for ordering of the water/pzac^{2-} ligands. Supplementary information contains further details of this disorder.

The framework structure of **II** is built up of a finite {Sm$_8$O$_{58}$} octamer constructed from two equivalent edge-sharing *SAPRS*-{Sm$_4$O$_{32}$} tetramers as shown in Figure 4(a), which are related by inversion and tied by 2×O3–C20–O4 of two equivalent TTHA^{6-} through two equivalent Sm1. The *SAPRS*-{Sm$_4$O$_{32}$} tetramer comprises four unique *SAPRS*-{SmO$_9$} motifs which are arranged in a repeating Sm1···Sm2···Sm3···Sm4 sequence and bridged by the OCO bridges of TTHA^{6-} (Table 2). Two ends of two successive octamers are further associated by the O26–C5–O27 bridge of TTHA^{6-}, leading to the formation of an infinite one-

dimensional chain in the [5 -10 7] direction. Distances between two successive Sm ions in the chain vary between 4.000(1) and 4.992(1) Å.

Although the $pzac^{2-}$ generated *in situ* is not involved in the construction of the one-dimensional chain, the ligand together with the fully deprotonated $TTHA^{6-}$ regulate the chain assembly (Figure 4(b)). As each $TTHA^{6-}$ binds three neighboring chains through seven Sm ions, every $pzac^{2-}$ bridges two neighboring Sm4 in the [1 0 0] direction. According to the calculation using PLATON [20], the chain assembly in **II** generates *ca.* 13.1% void volume which is over twice the void volume found for **Ia**. The free space comprises one-dimensional channels extending in the [1 0 0] direction. An effective size of the channel opening is *ca*. 4.98 (N1···N1) × 4.87 (O16···O18) $Å^2$, calculated from the shortest distances of the opposite atoms with the exclusion of the corresponding van der Waal radii. The channel is occupied by unbound water molecules, which are aligned along the channel direction through the hydrogen bonding interactions (Table 3).

In a similar fashion to **Ia** and **Ib**, as a result of the half $pzac^{2-}$ ion in the crystallographically-derived formula, $[Sm_8(TTHA)_4(pzac)_{0.5}(H_2O)_8]\cdot 4H_2O$, the framework of **II** is predicted to be negatively charged if only trivalent Sm ions are present. The existence of tetravalent Sm is extremely unlikely, although some of the BVS values deviate from the ideal value of three; BVS Sm1 = 3.13, Sm2 = 3.31, Sm3 = 3.45 and Sm4 = 3.35 or 3.45. Four of the $Sm-OH_2$ bond lengths about Sm4 in **II** lie in the range 2.42(1)-2.49(2) Å and the partially occupied O29B lies 2.63(2) Å from Sm4. According to literature, the significantly long Sm4-O29B suggests that O29B may be H_3O^+ rather than water [29,30-33]. Assuming the presence of H_3O^+, the chemical formula of **II** will be $[Sm_8(TTHA)_4(pzac)_{0.5}(H_3O)(H_2O)_{7.5}]\cdot 4H_2O$ which is chemically sensible. The existence of the two disordered components ($0.5pzac^{2-}$ and H_3O^+) in equal amounts gives weight to argument for charge balancing by the hydronium ion. This

assumption agrees well with the IR spectroscopy data (see supplementary information), revealing the characteristic absorption of H_3O^+ at 1800 cm^{-1} [25,26].

3.4. Structural description of IIIa and IIIb

Two isostructural compounds of general formula $[Ln_4(HTTHA)_2(SO_4)(H_2O)_4]\cdot4H_2O$, where Ln = Pr^{III} (**IIIa**) and Nd^{III} (**IIIb**), differ from the other compounds reported here in that compounds **IIIa** and **IIIb** include sulfate and the partially deprotonated HTTHA^{5-} anions. As these are isostructural, only the structure of **IIIa** will be presented. The asymmetric unit of **IIIa** consists of two distinct Pr ions, a whole molecule of HTTHA^{5-}, a disordered sulfate and water molecules as depicted in Figure 5. The sulfate bridges between Pr1 and Pr2^i (where i is the symmetry operator -x, -y, 1-z) account for 50 % of the Pr1 ions. It is not possible for every Pr1 to be coordinated by sulphate as this would lead to excessively close approach of symmetry generated counterparts. Thus for the remaining 50 % of sites one water molecule is coordinated to Pr1 (O13) and one to Pr2^i (O17) in place of bridging sulphate. Diagrams to illustrate this disorder are contained in the supplementary information.

Despite the complicated disorder, a nine-fold square-face tricapped trigonal prismatic *TPRS*-{PrO$_9$} coordination is adopted by Pr1 and Pr2 alike. While the *TPRS*-{PrO$_9$} of Pr1 is clearly characterized by eight O atoms (O2, O3, O4, 2×O5, O6, O9 and O11) from five HTTHA^{5-} and the substitutionally disordered O13, that of Pr2 is slightly more complicated. If the sulfate is not present, the *TPRS*-{PrO$_9$} unit is completed by seven O atoms (O1, O2, O3, O7, 2×O8 and O12) from three HTTHA^{5-} and two atoms (O17 and O18) from two distinct water molecules. Alternatively, if the water O17 is not present, the local geometry about Pr2 remains mostly the same but with the replacement of atom O17 with atoms O14 and O16 of the sulfate anion.

In a similar fashion to **Ia**, pairs of two equivalent *TPRS*-{PrO$_9$} motifs are fused through a common edge to make a *TPRS*-{Pr$_2$O$_{16}$} dimers, from which an infinite one-dimensional chain is constructed extending in the direction of [0 13 -20] with a regular alternation of Pr1 and Pr2 (Figure 6(a)). As the linkage between two equivalent Pr ions in two unique dimers are of the same type, *i.e.* 2×O6–C5–O5 for Pr1, and 2×O7–C7–O8 for Pr2, the fusion between the dimers of Pr1 and Pr2 occurs through three distinct bridges of the HTTHA^{5-}, *i.e.* O1–C1–O2, O4–C3–O3 and O11–C11–O12, as well as the sulfate. In addition to the bridging of the intra-chain Pr1 and Pr2, the disordered sulfate anion also links to an adjacent chain.

Rather than the close-packed assembly observed in **Ia**, the packing of the one-dimensional chains in **IIIa** occurs in an approximately square lattice as depicted in Figure 6(b). As the sulfate links two neighboring chains by the common 3.1110 bridging mode [34], the partially deprotonated HTTHA^{5-} anion connect four chains. Calculation in PLATON [20] suggests the void volume of 11.0%, which corresponds to a one-dimensional channel extending along *b* with an elliptical opening (Figure 6(c)). The effective size of the opening is 3.4 (O1···O1) × 6.3 (H4A···H4B) Å^2, approximated from the shortest distances between atoms located on the opposite channel wall. Located inside the channel are unbound water molecules, which form hydrogen bonds to the channel wall (Table 3).

In contrast to **Ia**, the crystallographically-derived formula for **IIIa** and **IIIb**, [Ln$_4$(HTTHA)$_2$(SO$_4$)(H$_2$O)$_4$]·4H$_2$O, does not suggest the presence of H$_3$O$^+$. Despite the BVS values of 3.39 calculated for Pr1, and 2.67 or 2.87 for Pr2, the crystallographically-dervied formula is consistent with Pr^{III} throughout.

3.5. Structural comparison and framework topologies

Compounds **Ia** (data collection at 150 K) and **Ib** (293 K) are isostructural, but distinct from **II** and the isostructural pair **IIIa** (150 K) and **IIIb** (293 K). Each of these compounds crystallizes in space group *P*-1. In comparison to the compounds in the isostructural series $[Ln_2(TTHA)(H_2O)_4]\cdot 9H_2O$ (Ln = Sm, Eu, Gd, Tb and Dy) crystallized in space group *C*2/*c* [13,14], the reduction in symmetry is apparent. This must result from the presence of secondary bridging ligands in **Ia**, **II** and **IIIa**, highlighting structural influence of these ligands. Furthermore, the presence of secondary bridging ligands increases the compactness of the frameworks. Compared with the three-dimensional channel of *ca.* 32 % void found in the open framework structure of $[Ln_2(TTHA)(H_2O)_4]\cdot 9H_2O$ [13,14], the one-dimensional channels of approximately one-third the volume define the frameworks of **II** and **IIIa**. The structure of **Ia** is a dense framework with no significant void space. The increase in framework compactness due to the presence of secondary ligand can be found likewise in the other lanthanide frameworks [35-37]. It can also be noted that the use of Sm (**II** and $[Sm_2(TTHA)(H_2O)_4]\cdot 9H_2O$ [14]) leads to different framework structures from those using Pr (**Ia** and **IIa**) and Nd (**Ib** and **IIb**) which provided isostructural crystals. This may contribute to the effect of lanthanide contraction [38-40].

   The frameworks reported here and those in the series of $[Ln_2(TTHA)(H_2O)_4]\cdot 9H_2O$ (Ln = Sm, Eu, Gd, Tb and Dy) [13,14], are constructed using similar dimeric building units, but differentiated by only a degree of compactness. While the dimer of the isostructural $[Ln_2(TTHA)(H_2O)_4]\cdot 9H_2O$ compounds emerges as an isolated motif leading to the open framework structure, the dimeric unit in **II** is condensed further to make an octamer which is then linked into an interrupted edge-sharing one-dimensional chain. In the frameworks of **Ia** and **IIIa**, these dimers are successively connected into the regular edge-sharing one-dimensional chains which are even more compact compared to the interrupted chain in **II**. The apparent deviation in chain formation of **Ia** from those of **II** and **IIIa** clearly originates from

dissimilarities in coordination modes displayed by the terminal carboxylate groups of the bridging $TTHA^{6-}$ and $HTTHA^{5-}$ ligands (Table 2). In addition to two common μ_2-η^1:η^2 and μ_2-η^1:η^1(*syn-syn*) modes of coordination, a diverse μ_2-η^1:η^1(*syn-anti*) and a monodentate μ_1-η^1:η^0 are exhibited by $TTHA^{6-}$ in **II** and $HTTHA^{5-}$ in **IIIa**, respectively.

Despite different modes of coordination adopted by the carboxylate, the conformations of the flexible $-N(CH_2COO)_2$ arms of $TTHA^{6-}$ and $HTTHA^{5-}$ in the reported compounds as well as $[Ln_2(TTHA)(H_2O)_4]\cdot 9H_2O$ (Ln = Sm, Eu, Gd, Tb and Dy) [13,14] are very similar as illustrated in Figure 7. As a pair of the $-N(CH_2COO)_2$ arms anchored onto the same N atom of the triazine core exhibits a *cis* conformation, the other two are in a *trans* fashion. Furthermore, every $-CH_2COO^-$ arm is arranged at almost right angle to the plane of the triazine core. The as-described spatial arrangement may be regarded as evidence for the preference of these *cis-trans-trans* conformation by the $TTHA^{6-}$ and $HTTHA^{5-}$ ligands in regulating the construction of lanthanide coordination polymers. Likewise, two flexible $-CH_2COO^-$ arms of $pzac^{2-}$ in each structures exhibit similar *trans* conformation with each $-CH_2COO^-$ arm allocated at almost right angle to the plane of the molecule.

In terms of framework topology, the frameworks of **Ia**, **II** and **IIIa** can be viewed as being evolved from the (4,4)-connected cooperite (**pts**) framework of the isostructural $[Ln_2(TTHA)(H_2O)_4]\cdot 9H_2O$ compounds [13,14]. The frameworks of **Ia**, **II** and **IIIa** can be simplified to **pts** net by excluding the secondary $pzac^{2-}$ and sulfate ligand, as depicted in Figure 8. In this case, the dimeric unit and $TTHA^{6-}$ ligand act as the 4-connected nodes of different geometries, *i.e.* a square and a distorted tetrahedral, respectively. Both of these geometries are the basic for **pts** net [34]. The inclusion of $pzac^{2-}$ and sulfate nonetheless leads to a disruption of the **pts** nets. Since the coordination of $pzac^{2-}$ to the *TPRS*-$\{Pr_2O_{16}\}$ dimer in **Ia** and the *SAPRS*-$\{Sm_2O_{16}\}$ dimer in **II** results in the formation of the other infinite one-dimensional chains, the **pts** nets of **Ia** and **II** can be therefore viewed as being cross-linked by

these chains. The sulfate ions in **IIIa**, on the other hand, form the other uninodal 4-connected Shubnikov (**sql**) tetragonal plane net laying in the crystallographic *ab* plane. In this case, if site disorder of the sulfate is ignored and the anion acts as the 4-connected square node with the *TPRS*-$\{Pr_2O_{16}\}$ dimer as a 2-connected linker, net of **IIIa** can be viewed as the **pts** net which is intertwined by the 4-connected **sql** net. The **sql** net is one of the most familiar two-dimensional nets, which has the highest occurrence in the construction of the higher dimensional nets [41].

4. Conclusion

In conclusion, a series of new lanthanides coordination polymers have been hydrothermally synthesized by using deprotonated H_6TTHA as the primary ligands with either $pzac^{2-}$ or sulfate as the secondary ligand. The crystallographic disorder is common for these small ligands. The framework structures of the title compounds are similarly built up from the edge-shared lanthanide dimeric units, and are diversified by differences in coordination modes of the carboxylate. Despise varying degree of protonation in H_6TTHA, the ligand shows preferences toward the μ_2-η^2:η^1 and μ_2-η^1:η^1 modes of coordination and the *cis-trans-trans* conformation for the flexible $-N(CH_2COO)_2$ arms. The presence of the secondary ligands introduces compactness to the derived frameworks compared to those comprising only the deprotonated H_6TTHA. In terms of topology, these secondary bridging ligands can be viewed as the disruptive factors to the **pts** net observed for the $[Sm_2(TTHA)(H_2O)_4] \cdot 9H_2O$ [14].

Program, the Science Achievement Scholarship of Thailand, and the Graduate School of Chiang Mai University for Graduate Scholarships.

Supplementary Material

Crystallographic data (excluding structure factors) for the title compounds have been deposited with the Cambridge Crystallographic Data Centre; CCDC 1023509 (**Ia**), 1023510 (**II**) and 1023511 (**IIIa**). Copies of this information may be obtained free of charge from The Director, CCDC, 12 Union Road, Cambridge CB2 1EZ, UK (fax: +44 1223 336033; e-mail: deposit@ccdc.cam.ac.uk). NMR data of the employed ligand, and information on the crystallographic disordering, powder X-ray diffraction and IR spectroscopy are provided as supplementary information.

References

[1] M. Fujita, D. Oguro, M. Miyazawa, H. Oka, K. Yamaguchi, K. Ogura, *Nature* 378 (1995) 469.

[2] X. Liang, F. Zhang, H. Zhao, W. Ye, L. Long, G. Zhu, *Chem. Commun*. 50 (2014) 6513.

[3] J. Li, T. Sheng, S. Bai, S. Hu, Y. Wen, R. Fu, Y. Huang, Z. Xue, X. Wu, *Inorg. Chem*. 53 (2014) 289.

[4] Q. Tang, S. Liu, Y. Liu, D. He, J. Miao, X. Wang, Y. Ji, Z. Zheng, *Cryst. Eng. Comm*. 16 (2014) 2188.

[5] S.N.G. Acharya, R.S. Gopalan, G.U. Kulkarni, K. Venkatesan, S. Bhattacharya, *Chem. Commun*. 15 (2000) 1351.

[6] F.H. Allen, *Acta Cryst*. B58 (2002) 380.

[7] Q.-L. Zhu, T.-L. Sheng, R.-B. Fu, S.-M. Hu, L. Chen, C.-J. Shen, X. Ma, X.-T. Wu, *Chem. Eur. J.* 17 (2011) 3358.

[8] Q. Zhu, T. Sheng, C. Tan, S. Hu, R. Fu, X. Wu, *Inorg. Chem.* 50 (2011) 7618.

[9] X. Jiang, G. Yan, Y.-H. Liao, C.-X. Huang, H. Xia, *Inorg. Chem. Commun.* 14 (2011) 1924.

[10] X. Jiang, L. Lin, Y.-F. Zhu, H. Xia, *Transition Met. Chem.* 36 (2011) 901.

[11] X. Jiang, H. Xia, Y.-F. Zhu, C.-X. Huang, Y.-H. Liao, *Z. Anorg. Allg. Chem.* 637 (2011) 2273.

[12] X. Jiang, B. Tao, H. Xia, G.-Y. Liao, *Cryst. Eng. Comm.* 14 (2012) 3271.

[13] Q. Zhu, T. Sheng, R. Fu, S. Hu, J. Chen, S. Xiang, C. Shen, X. Wu, *Cryst. Growth Des.* 9 (2009) 5128.

[14] S. Surinwong, B. Yotnoi, T.J. Prior, A. Rujiwatra, *J. Inorg. Organomet. Polym.* 23 (2013) 1032.

[15] X.-J. Kong, G.-L. Zhuang, Y.-P. Ren, L.-S. Long, R.-B. Huang, L.-S. Zheng, *Dalton Trans.* 10 (2009) 1707.

[16] W. Karuehanon, W. Fantuenha, A. Rujiwatra, M. Pattarawarapan, *Tetrahedron Lett.* 53 (2012) 3486.

[17] J. de Meulenaer, H. Tompa, *Acta Cryst.* 19 (1965) 1014.

[18] G.M. Sheldrick, *Acta Cryst.* A64 (2008) 112.

[19] L.J. Farrugia, *J. Appl. Cryst.* 32 (1999) 837.

[20] A.L. Spek, *J. Appl. Cryst.* 36 (2003) 7.

[21] V.S. Urusov, I.P. Orlov, *Crystallogr. Rep.* 44 (1999) 686.

[22] S.A. Cotton, V. Franckevicius, M.F. Mahon, L.L. Ooi, P.R. Raithby, S.J. Teat, *Polyhedron* 25 (2006) 1057.

[23] J. Cepeda, R. Balda, G. Beobide, O. Castillo, J. Fernández, A. Luque, S. Pérez-Yáñez, P. Román, D. Vallejo-Sánchez, *Inorg. Chem.* 50 (2011) 8437.

[24] M. Feyand, C. Näther, A. Rothkirch, N. Stock, *Inorg. Chem.* 49 (2010) 11158.

[25] I. Xueref, F. Dominé, *Atmos. Chem. Phys.* 3 (2003) 1779.

[26] J. D. Russell, A.R. Fraser, *Clays Clay Miner.* 19 (1971) 55.

[27] X.-L. Sun, B.-X. Shen, S.-Q. Zang, C.-X. Du, *Cryst. Eng. Comm.* 15 (2013) 5910.

[28] R. Janicki, A. Mondry, *Eur. J. Inorg. Chem.* 19 (2013) 3429.

[29] P. Wang, R.-Q. Fan, X.-R. Liu, L.-Y. Wang, Y.-L. Yang, W.-W. Cao, B. Yang, W. Hasi, Q. Su, Y. Mu, *Cryst. Eng. Comm.* 15 (2013) 1931.

[30] J.-P. Wang, J.-W. Zhao, X.-Y. Duan, J.-Y. Niu, *Cryst. Growth Des.* 6 (2006) 507.

[31] Q. Liu, S.-Z. Ge, J.-C. Zhong, Y.-Q. Sun, Y.-P. Chen, *Dalton Trans.* 42 (2013) 6314.

[32] D. Aguilà, L.A. Barrios, V. Velasco, L. Arnedo, N. Aliaga-Alcalde, M. Menelaou, S.J. Teat, O. Roubeau, F. Luis, G. Aromí, *Chem. Eur. J.* 19 (2013) 5881.

[33] P. Wang, R.-Q. Fan, Y.-L. Yang, X.-R. Liu, P. Xiao, X.-Y. Li, W. Hasi, W.-W. Cao, *Cryst. Eng. Comm.* 15 (2013) 4489.

[34] B. Yotnoi, N. Meundaeng, A. Rujiwatra, *Synth. React. Inorg. Met.-Org. Chem.* 44 (2014) 1373.

[35] F. Zhang, X.-T. Huang, Y.-Y. Tian, Y.-X. Gong, X.-Y. Chen, J.-J. Lin, D.-S. Lu, Y.-L. Zhang, R.-H. Zeng, S.-R. Zheng, *J. Coord. Chem.* 66 (2013) 2659.

[36] Z.-J. Xiahou, Y.-L. Wang, Q.-Y. Liu, L-Q. Li, L.-J. Zhou, *J. Coord. Chem.* 66 (2013) 2910.

[37] M. Yu, X. Wang, M. Hu, J. Coord. Chem. 68 (2015) 520.

[38] X. Fang, L.-M. Cai, Y.-C. Shao, M.-J. Lin, *J. Coord. Chem.* 67 (2014) 3541.

[39] Q. Cheng, W.-Y. Huang, O.-H. Huang, Y.-J. Xiong, J.-F. Fang, Y. Li, F.-F. Zhu, S.-T. Yue, *J. Coord. Chem.* 68 (2015) 1980.

[40] H. Xie, G. Lu, *J. Coord. Chem.* 68 (2015) 1800.

[41] D.S. Li, Y.-P. Wu, J. Zhao, J. Zhang, J.Y. Lu, *Coord. Chem. Rev.* 261 (2014) 1.

Table 1. Crystallographic data and refinement details.

	Ia	Ib	II	IIIa	IIIb
Formula	$C_{34}H_{29}N_{13}O_{35}Pr_4$	$C_{34}H_{29}N_{13}O_{35}Nd_4$	$C_{64}H_{53}N_{25}O_{63}Sm_8$	$C_{30}H_{30}N_{12}O_{36}Pr_4S$	$C_{30}H_{24}N_{12}O_{36}Nd_4S$
Formula weight	1743.34	1756.66	3382.11	1730.36	1737.63
Crystal setting	Triclinic, P-1	Triclinic, P-1	Triclinic, P-1	Triclinic, P-1	Triclinic, P-1
a (Å)	9.9245(12)	9.9171(15)	11.4156(9)	9.7887(9)	9.7547(4)
b (Å)	11.0004(14)	11.0222(17)	13.7226(10)	10.0556(10)	10.0569(5)
c (Å)	13.8484(16)	13.819(2)	17.4115(14)	12.4566(11)	12.4275(6)
α (°)	77.599(10)	77.370(4)	76.985(6)	92.514(8)	92.5470(10)
β (°)	79.108(9)	78.795(4)	82.578(6)	91.623(7)	91.7890(10)
γ (°)	66.395(9)	66.102(4)	88.768(6)	91.495(8)	91.3620(10)
V (Å^3)	1344.1(3)	1338.1(4)	2635.1(4)	1224.0(2)	1216.98(10)
Z	1	1	1	1	1
T (K)	150(2)	293(2)	150(2)	150(2)	293(2)
ρ_{calc} (g·cm^{-3})	2.153	2.180	2.131	2.348	2.371
μ (mm^{-1})	3.675	3.931	4.497	4.072	4.363
θ range (°)	2.86-34.71	2.75-34.82	2.55-34.89	2.55-34.70	2.03-30.65
λ (Mo $K\alpha$) (Å)	0.71073	0.71073	0.71073	0.71073	0.71073
R_{int}	0.0644	0.0404	0.0800	0.0432	0.0144
Collected reflection	11388	5506	11493	5901	7357
unique reflections	8265	4378	8030	4910	6537
no. of parameters	419	410	721	392	395
R, Rw (I>2σ(I))	0.0484, 0.1138	0.0700, 0.1654	0.0603, 0.1529	0.0374, 0.0987	0.0336, 0.0974
R, Rw (all data)	0.0755, 0.1251	0.0898, 0.1818	0.0915, 0.1693	0.0482, 0.1034	0.0398, 0.1070
GOF on F^2	1.059	1.117	1.031	1.045	1.144

Table 2. List of coordination modes observed for each carboxylate and the corresponding bridged lanthanides in **Ia**, **II** and **IIIa**.
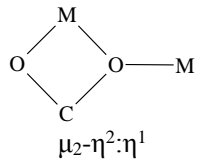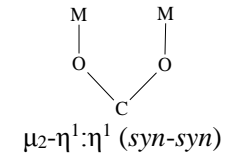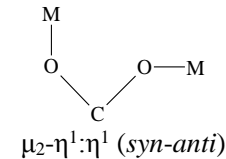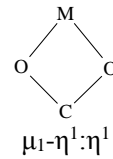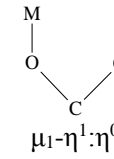
Coordination modes of –OCO

	μ_2-η^2:η^1	μ_2-η^1:η^1 (*syn-syn*)	μ_2-η^1:η^1 (*syn-anti*)	μ_1-η^1:η^1	μ_1-η^1:η^0
Ia					
μ_7-η^{16} TTHA^{6-}	O1–C1–O2 (Pr1:Pr1)	O9–C9–O10 (Pr1:Pr2)			
	O3–C3–O4 (Pr2:Pr2)	O11–C11–O12 (Pr1:Pr1)			
	O5–C5–O6 (Pr1:Pr2)				
	O7–C7–O8 (Pr1:Pr2)				
pzac^{2-}				O14–C16–O15	
II					
μ_7-η^{16} TTHA^{6-}	O3–C20–O4 (Sm1:Sm1)	O13–C16–O21 (Sm2:Sm3)			
	O14–C22–O15 (Sm1:Sm3)	O19–C18–O23 (Sm3:Sm4)			
	O7–C24–O11 (Sm1:Sm2)				
	O22–C26–O24 (Sm3:Sm4)				
μ_7-η^{15} TTHA^{6-}	O1–C1–O2 (Sm1:Sm2)	O8–C9–O9 (Sm1:Sm2)	O26–C5–O27		
	O18–C3–O20 (Sm3:Sm4)	O12–C11–O17 (Sm2:Sm3)	(Sm4:Sm4)		
	O10–C7–O16 (Sm2:Sm3)				
pzac^{2-}				O28–C31–O29A	
IIIa					
μ_8-η^{15} TTHA^{6-}	O1–C1–O2 (Pr1:Pr2)	O11–C11–O12 (Pr1:Pr2)			O9–C9–O10
	O3–C3–O4 (Pr1:Pr2)				
	O5–C5–O6 (Pr1:Pr1)				
	O7–C7–O8 (Pr2:Pr2)				

Table 3. List of hydrogen bonding interactions and geometries (bond lengths in Å and angle in °).

Ia[†]				II[§]				IIIb[‡]			
D–H···A	H···A	D···A	∠D–H···A	D–H···A	H···A	D···A	∠D–H···A	D–H···A	H···A	D···A	∠D–H···A
O1···O1W	-	2.721(4)	-	O9···O1W	-	2.846(8)	-	O1···O1WA[i]	-	2.90(2)	
O1···O1W[i]	-	2.721(4)	-	O9···O1W[i]	-	2.846(8)	-	O1···O1WB[i]	-	2.82(2)	
O10···O1W	-	2.800(5)	-	O11···O1W	-	2.923(8)	-	O7···O1WA[i]	-	2.79(2)	
O10···O1W[i]	-	2.800(5)	-	O11···O1W[i]	-	2.923(8)	-	O7···O1WB[i]	-	2.87(2)	
O1···O2W	-	3.290(6)	-	O15···O1W	-	2.705 (1)	-	O18···O1WA[ii]	-	2.82(2)	
O2···O2W[ii]	-	3.280(8)	-	O15···O1W[i]	-	2.705(1)	-	O18···O1WB[ii]	-	2.65(2)	
O5···O2W	-	2.870(7)	-	O16···O2W[ii]	-	2.866(7)	-	O1WA···O1WB[iii]	-	3.19(3)	
O11···O2W	-	3.26(1)	-	O16···O2W[iii]	-	2.866(4)	-	O1WB···O1WA[iii]	-	3.19(3)	
O2W···O2W[iii]	-	2.856(7)	-	O18···O2W[ii]	-	2.893(7)	-	O10-H10···O13	2.42	3.087(9)	140
O4···O3W[iv]	-	2.78(1)	-	O18···O2W[iii]	-	2.893(7)	-	O10-H10···O15	1.89	2.64(2)	153
O7···O3W[iv]	-	2.80(1)	-	O19···O2W[ii]	-	2.757(9)	-	O18-H18A···O10[iv]	2.04(5)	2.812(9)	151(6)
O13···O3W[v]	-	2.61(1)	-	O19···O2W[iii]	-	2.757(9)	-	O18-H18B···O17[iv]	1.85(6)	2.61(1)	152(6)
O3W···O3W[vi]	-	3.16(3)	-	O11···O3W	-	2.89(1)	-	C2-H2A···O6	2.47	3.350(6)	151
C2-H2B···O14[ii]	2.40	3.10(1)	128	O3W···O3W[iv]	-	2.87(1)	-	C6-H6B···N6[v]	2.43	2.797(7)	102
C12-H12A···O2W[i]	2.32	3.270(9)	168	C2-H2B···O13[iii]	2.51	3.34(1)	143	C10-H10B···O4[vi]	2.49	3.252(8)	135
				C12-H12A···O3W[iv]	2.41	3.35(2)	162	C12-H12B···O6	2.50	3.261(6)	135
				C23-H23B···O28	2.50	3.21(1)	130				
				C33-H33B···O29A	2.58	3.090(3)	112				

[†]Symmetry codes: (i) 1-*x*, 1-*y*, 1-*z*; (ii) 1-*x*, 2-*y*, 1-*z*; (iii) -*x*, 2-*y*, 1-*z*; (iv) 1-*x*, 1-*y*, 2-*z*; (v) -1+*x*, *y*, *z*; (vi) -*x*, 1-*y*, 2-*z*.

[§]Symmetry codes: (i) 1-*x*, 1-*y*, -*z*; (ii) -1+*x*, *y*, *z*; (iii) 1-*x*, 1-*y*, 1-*z*; (iv) 2-*x*, 1-*y*, -*z*.

[‡] Symmetry codes: (i) -*x*, 1-*y*, 1-*z*; (ii) -1+*x*, *y*, *z*; (iii) -1-*x*, 1-*y*, 1-*z*; (iv) *x*, 1+*y*, *z*; (v) -*x*, -*y*, 2-*z*; (vi) -*x*, 1-*y*, 2-*z*.

Figure captions

Scheme 1. Diagrammatic illustrations of (a) H_6TTHA and (b) H_2pzac.

Figure 1. View of the asymmetric unit of **Ia** with atoms drawn as 60% thermal ellipsoids. The hydrogen atoms are omitted for clarity. Symmetry codes: (i) 1-x, 1-y, 2-z (ii) 1-x, 2-y, 1-z.

Figure 2. Polyhedral representations showing (a) the edge-sharing of $SAPRS$-$\{PrO_9\}$ and $SAPRS$-$\{PrO_{10}\}$ units to form the one-dimensional chain, and (b) the hexagonal close-packing of these chains in **Ia**.

Figure 3. View of the asymmetric unit of **II** with atoms drawn as 60% thermal ellipsoids. The hydrogen atoms are omitted for clarity. Symmetry codes: (i) 1-x, 2-y, -z (ii) 2-x, 1-y, 1-z.

Figure 4. Polyhedral representations showing (a) the edge-sharing octamer and the one-dimensional channel extending in the direction of a, and (b) the packing of these chains in **II**.

Figure 5. View of the asymmetric unit of **IIIa** with atoms drawn as 60% thermal ellipsoids. The hydrogen atoms are omitted for clarity. Symmetry codes: (i) -x, -y, 1-z (ii) -x, -y, 2-z.

Figure 6. Polyhedral representations showing (a) the formation of one-dimensional chain in **IIIa**, (b) the packing of these chains in a square lattice-like, and (c) the one-dimensional channel extending in the direction of b.

Figure 7. Spatial arrangements of the flexible hexacarboxylate arms of TTHA^{6-} in **Ia** (a) and **II** (b, c), and of HTTHA^{5-} in **IIIa** (d). Hydrogen atoms are omitted for clarity.

Figure 8. Topological representations of the disrupted nets evolved from the (4,4)-connected **pts** net in (a) **Ia** (b) **II** and (c) **IIIa**.